1

Magnets for Small-Scale and Portable NMR

Bernhard Blümich[1], *Christian Rehorn*[1], *and Wasif Zia*[2]

[1] *RWTH Aachen University, Institut für Technische und Makromolekulare Chemie, Worringerweg 2, 52074 Aachen, Germany*
[2] *Sir Peter Mansfield Imaging Center, University of Nottingham, United Kingdom*

1.1 Introduction

Nuclear magnetic resonance (NMR) exploits the resonance of the precessing motion of nuclear magnetization in magnetic fields [1, 2]. From the measurement methodology, three groups of common techniques of probing resonance can be assigned: those employing forced oscillations, free oscillations, and interferometric principles [3]. In either case, the sensitivity depends on the strength of the nuclear magnetic polarization, which, in thermodynamic equilibrium at temperatures higher than few degrees above absolute zero, is in good approximation proportional to the strength of the magnetic field. In recognition of this fact, one guideline in the development of NMR magnets has always been to reach high field strength. The highest field strength of temporally stable magnetic fields today is achieved with superconducting electromagnets. This is why most standard NMR instruments used for NMR spectroscopy in chemical analysis and magnetic resonance imaging (MRI) in medical diagnostics employ superconducting magnets cooled to the low temperature of boiling helium with cryogenic technology.

Another force driving the development of high-field magnets is that the frequency range of the chemical shift is also proportional to the field strength. The wider the frequency range, the more complicated are the molecules that can be analyzed by NMR spectroscopy. High magnetic fields are most crucial in structural biology [4]. In chemistry and biology, molecules are mostly studied in liquid solutions. The NMR spectra of such molecules can show hundreds of narrow resonance lines, which can be better separated at high field, provided the magnetic field is sufficiently homogeneous. Else, the resonance lines from different volume elements of the sample shift and the sum spectrum measured from all volume elements show small and broad peaks instead of narrow and tall peaks (Figure 1.1c vs e). In either case, the peak area is determined by the number of nuclei resonating in the given frequency range, and the resonance frequency ν is determined by the strength B of the magnetic field, which is

Micro and Nano Scale NMR: Technologies and Systems, First Edition.
Edited by Jens Anders and Jan G. Korvink.

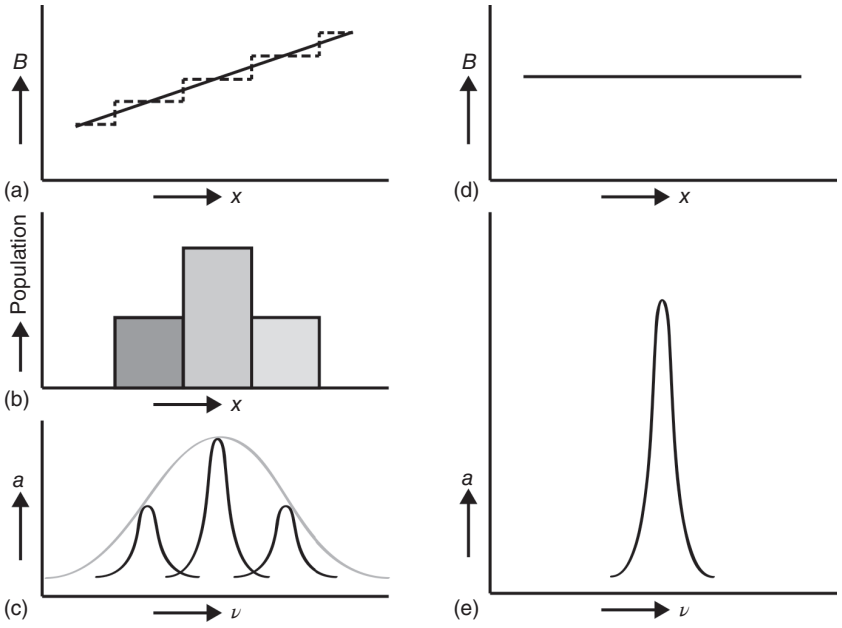

Figure 1.1 NMR in inhomogeneous and in homogeneous fields. (a) Magnetic field strength B linearly varying with pixel position x. (b) Three pixels containing different numbers of NMR-active nuclei at different positions x. (c) NMR spectrum observed in an inhomogeneous field (gray). For the case that the magnetic field B is homogeneous across each pixel (broken lines in a), the peak integral is proportional to the total magnetization at each pixel (black). (d) Spatially homogeneous magnetic field. (e) In a homogeneous field, the resonance signals from each pixel sum up at the same frequency.

experienced by the nuclei (Figure 1.1),

$$2\pi\nu = \gamma B \tag{1.1}$$

where γ is the gyromagnetic ratio of the nucleus under observation.

In NMR spectroscopy, the frequency range of the signal-bearing nuclei depends on the nuclide. Small-scale instruments use permanent magnets with low field strengths so that their sensitivity is low, unless the nuclear polarization is enhanced by hyperpolarization methods [3, 5]. The most sensitive, stable NMR nuclei are ^{1}H and ^{19}F. ^{1}H is the most abundant element in the universe and is found in water and organic matter. It has a frequency range of $\Delta\nu = 12\ \text{ppm} \times \nu$, where ppm denotes 10^{-6}. ^{19}F, on the other hand, is similarly sensitive but with a much wider frequency range of $\Delta\nu / \nu = 400\,\text{ppm}$. It is frequently encountered in pharmaceutical compounds and can be detected against a ^{1}H signal background due to its resonance frequency being 40 MHz at $B = 1\,\text{T}$ versus 42 MHz for ^{1}H. Thus, both types of nuclei are of great interest also for miniature NMR devices.

To resolve individual resonance lines within these frequency ranges, the magnetic field needs to be homogeneous with an accuracy of 0.1–0.01 ppm across the sample extension for ^{1}H and with a factor of about 10 less for ^{19}F (Fig. 1.1d). This magnetic field homogeneity defines a design goal for spectroscopy-grade permanent NMR magnets. In terms of the magnetic field varying linearly along the space direction x across a 5 mm diameter sample, the field gradient

$G = \mathrm{d}B/\mathrm{d}x$ should consequently be smaller than for $0.5 \times 10^{-4}\,\mathrm{T/m}$ for ^{1}H (Figure 1.1a). Note that this is two orders of magnitude less than the minimum gradient required to resolve structures in NMR imaging of soft matter at the 1 mm scale at 1 T where one deliberately applies linear magnetic field profiles across the object to measure projections of the magnetization density in terms of NMR spectra.

If the field inhomogeneity is higher, NMR spectra cannot be resolved, but NMR relaxation can still be measured by echo techniques [1, 2, 6]. In fact, NMR relaxometry experiments can be executed in arbitrarily inhomogeneous magnetic fields, where the NMR signal is spread over wide frequency ranges (Fig. 1.1c). The signal amplitude is then limited by the excitation bandwidth, which in turn is determined by the duration t_p of the excitation pulse and the resonance characteristics of the transmit/receive electronics. For example, to excite all spins across the diameter of a 5 mm sample tube with a 10 µs excitation pulse, the average field gradient for ^{1}H relaxometry should be less than 0.5 T/m. Although NMR spectroscopy experiments are in demand for chemical identification, NMR relaxometry experiments are employed for characterizing physical properties of condensed liquids and solids such as crude oil, foodstuff, plants, and polymers [6, 7] as well as for identifying relaxation agents with chemical functionality, which bind to markers of disease in biological extracts [8–12]. Depending on their use, NMR magnets are consequently categorized into magnets with high field homogeneity for both NMR spectroscopy and relaxometry at the same time and magnets with lesser homogeneity, which are suitable for NMR imaging and relaxometry or NMR relaxometry only.

1.2 Compact Permanent Magnets

1.2.1 Types of Permanent Magnets

A big advantage of using permanent magnets over superconducting devices is their portability and lower weight. On the downside, they usually provide less homogeneity and lower field [13]. Although NMR relaxation can be measured in inhomogeneous fields, sample size, inhomogeneity, and radio frequency (RF) pulse width commonly define two limiting cases. In the first case, the magnetization in each voxel of the sample can be exited with an RF pulse. In the second case, only a subset of all voxels can be excited. In this case, the RF pulse is said to be selective because the spread in resonance frequencies from all voxels in the object caused by the field inhomogeneity is larger than the excitation bandwidth. Typically, this situation is encountered in unilateral stray-field NMR, where a small NMR sensor is placed near a large object (Figure 1.2a), and the stray magnetic field decays with distance into the object along with the NMR resonance frequency. A popular example of such a sensor is the NMR-MOUSE [14], which typically operates at a magnetic field strength in the vicinity of 0.5 T with a gradient of 10–20 T/m depending on the size of the device. Stray-field sensors are employed for nondestructive testing because the object can be arbitrarily large [15].

The average gradient of the NMR-MOUSE is more than one order of magnitude larger than the gradient tolerable for NMR relaxometry with nonselective

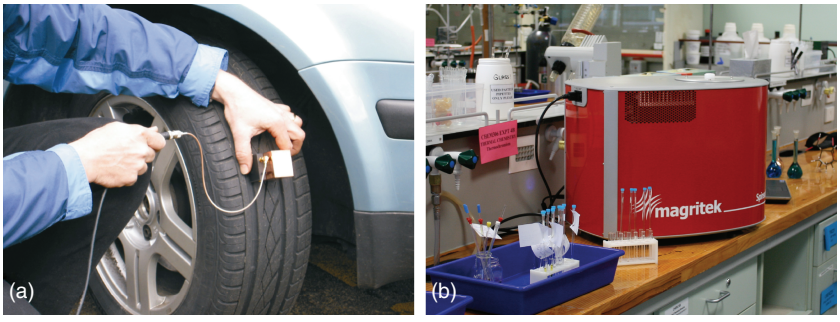

Figure 1.2 Types of compact NMR magnets. (a) A stray-field magnet is placed close to the object, here a car tire, for analysis of material properties. (b) A center-field magnet accommodates the sample inside, here one of the 5 mm diameter sample tubes (foreground) containing the sample solution. The magnet is the most voluminous component of the NMR spectrometer (red). The sample tube is inserted into the magnet from the top.

excitation of typical 5 mm diameter samples. Magnets with low gradients suitable for nonselective relaxometry, imaging, and spectroscopy are easier to construct when they surround the object. This, however, limits the object diameter because the object needs to be inserted into an opening of the magnet body (Figure 1.2b). In contrast to stray-field magnets, such magnets are referred to as center-field magnets in the following. If the object size exceeds the dimensions of the magnet bore, samples need to be drawn from the object, a procedure common in chemical analysis of molecules in solution by NMR spectroscopy.

The arguments specifying the tolerable average field gradient across the sample also relate to the quality factor of the resonance circuit, which detects the nuclear induction signal. It is defined as the ratio of the resonance frequency ω over the detection bandwidth as $Q = \omega/\Delta\omega$, where $\Delta\omega$ is of the order of the inverse excitation pulse width t_p, $\Delta\omega \approx 1/t_p$. A high-quality factor is desirable for high sensitivity of signal detection, especially at very low field [16]. On the other hand, it limits the detection bandwidth $\Delta\omega = \omega/Q$ (Figure 1.3). The better the field homogeneity, the smaller the spectral width of the detected signal in relaxometry experiments and the higher the value of Q that can be set in the detection circuit. In most relaxometry magnets, the quality factor of the resonance circuit is

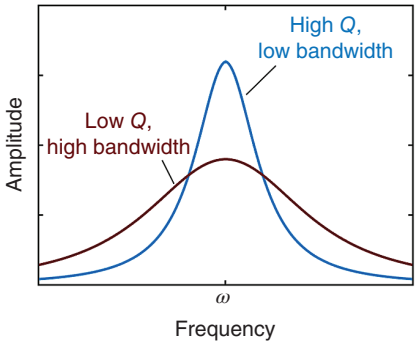

Figure 1.3 Resonance curves illustrating the relation between quality factor Q and excitation bandwidth $\Delta\omega$ in a resonance circuit. The larger the quality factor, the lower is the observed excitation bandwidth relative to the resonance frequency ω.

optimized to low values so that the excitation bandwidth remains only a function of the pulse length t_p [17].

1.2.2 Stray-Field Magnets

1.2.2.1 Classification

Stray-field magnets require caution in handling because on their active side, a strong stray magnetic field emanates and attracts magnetic objects. The opposite side can be shielded by guiding the flux through a ferromagnetic yoke. There are two principle ways in which the stray magnetic field $\boldsymbol{B}_0$ flooding the object can be oriented. These are parallel to the magnet surface (Figure 1.4a,c) and perpendicular to it (Figure 1.4b,d). The RF coil has then to be designed accordingly so that the magnetic RF field $\boldsymbol{B}_1$ is orthogonal to $\boldsymbol{B}_0$ in a large volume.

The sensitive volume resulting from the profiles of $\boldsymbol{B}_0(r)$ and $\boldsymbol{B}_1(r)$ is ill defined in the general case. Nevertheless, two limiting geometries are favored, one in which the stray magnetic field is parallel to the magnet surface (Figure 1.4c) and one in which the field is essentially perpendicular to the surface forming a sweet

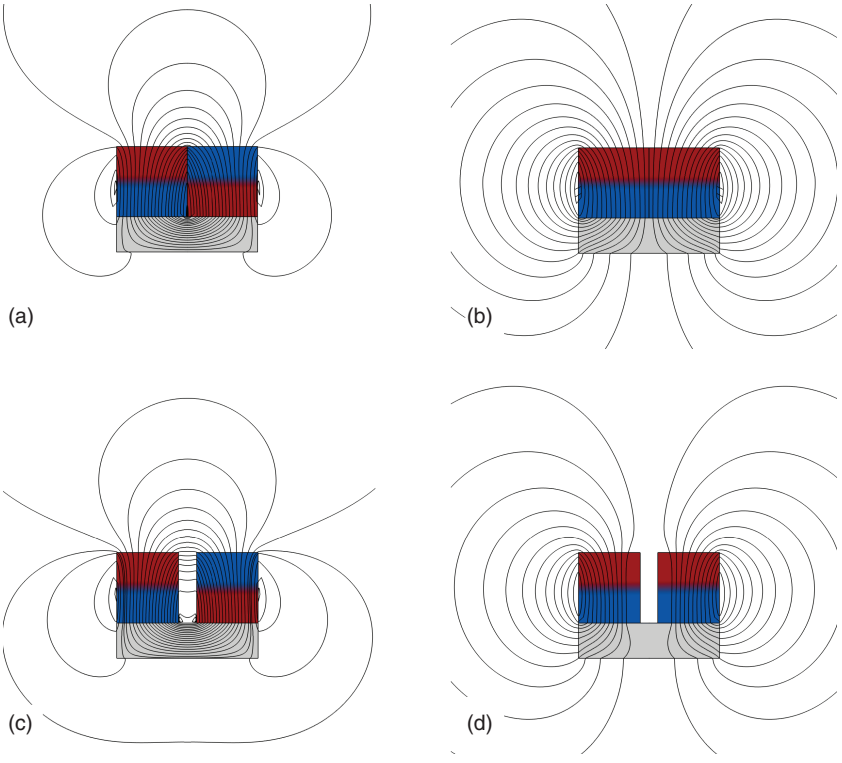

Figure 1.4 Compact stray-field NMR magnets with iron yokes (gray) to shield the stray field on the bottom side. The object (not shown) approaches the sensor from the top. The stray field emanating from the top passes through the object with its field lines either parallel to the magnet surface (a,c) or perpendicular to it (b,d). Gaps are a simple way to shim the field by bending the field lines adjacent to the gap (c,d).

spot [8, 18–20] of improved homogeneity in a volume distant from the magnet surface (Figure 1.4d). The first geometry collects the signal from a thin slice parallel to the sensor surface and the second one from a more bulky volume. In either case, the stray magnetic field needs to be shimmed to the desired level of homogeneity in the sensitive volume.

Shimming denotes the deformation of magnetic field lines in order to decrease or eliminate existing gradients. A simple way to shim the field is by introducing gaps into a dense array of magnet blocks (Figure 1.4c,d) [21, 22]. This distorts the field lines at the expense of reducing their density corresponding to the magnitude of the stray magnetic field. Alternatively, magnets can be placed into the gaps to enhance or attenuate the shimming efficiency, or suitably shaped iron pole shoes can be placed on top of the sensor surface. The positions of these magnets can then be fine-tuned. Stray-field magnets that have been realized for NMR measurements have been surveyed in the literature [15, 17, 23]. Typical distances of the sensitive volume from the sensor surface are a few millimeters to a few centimeters at field strengths of 0.1–0.5 T with gradients of 0.1–20 T/m. As a rule of thumb, the smaller the field strength, the lower is the gradient. Moreover, the gradient along the depth direction approximately scales with the inverse square of the magnet surface at the object side.

1.2.2.2 Magnets for 1D and 2D Imaging

Stray-field magnets for 2D imaging in planes parallel to the sensor surface and 1D imaging in the depth direction equivalent to depth profiling are constructed along the same design principle: both employ a flat sensitive slice parallel to the surface of the magnet. Such a slice is most easily obtained with an array of four magnets positioned on an iron yoke with gaps between the magnets to flatten the field lines at a given distance above the magnet surface (Figure 1.5a). This array can be understood as two of the magnet arrays shown in Figure 1.4c placed parallel to each other with a narrow gap in between. It is known as the Profile NMR-MOUSE [21]. With both gaps properly adjusted, a flat slice of constant magnetic field is defined at a fixed distance above the magnet surface with a constant gradient pointing toward the magnet surface. The slice diameter is defined by the dimension of the RF coil and varies between 4 mm and 4 cm.

For planar imaging, the extension of the sensitive slice defines the field of view, which is divided into pixels with the help of additional pulsed field gradients by imaging with phase-encoding techniques [25]. Depending on the field gradient of the sensor and the measurement parameters, the slice thickness is typically between 100 and 300 µm. Commercial stray-field sensors specify the maximum spatial resolution to 10 µm. In exceptional situations, 3 µm and less have been achieved [21, 24]. For comparison, slices in slice-selective medical imaging are a few millimeters thick. Therefore, 2D planar imaging with stray-field sensors lacks sensitivity and has never passed the proof-of-principle stage [25, 26]. On the other hand, the integral signal from the thermal nuclear ^{1}H magnetization located in such a thin but wide sensitive slice is in most cases good enough to acquire signal from solid and soft matter for nondestructive materials testing and depth profiling. Small versions of the Profile NMR-MOUSE have been built with dimensions of 56 mm × 75 mm × 44 mm weighing 500 g (MiniMOUSE) and

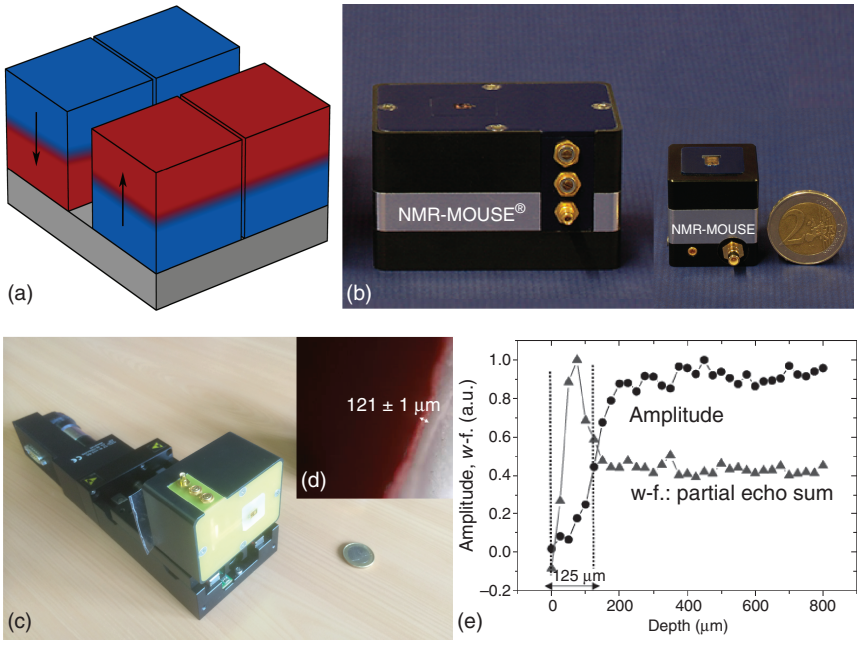

Figure 1.5 Stray-field magnet with a planar sensitive slice. (a) Arrangement of magnets on an iron yoke. Both gaps are adjusted to define a planar region of constant magnetic field at a fixed distance above the magnet. (b) MiniMOUSE (left) and MicroMOUSE (right) fitted with a microcoil and suitable for depth profiling. (c) MiniMOUSE mounted on an optical displacement table to scan a 1 mm distance with 0.2 µm precision. The sensor has a gradient of 68 T/m and a resonance frequency of 17.1 MHz. (d) Photo of a painted car fender section showing the paint layer. (e) Depth profile through the paint layer of the car fender. (Adapted from Ref. [24].)

28 mm × 28 mm × 31 mm weighing 80 g (MicroMOUSE) (Figure 1.5b) [24, 27]. In situations where the dimensions of the sensor are that small, microcoils were utilized to increase sensitivity [28, 29].

To acquire a depth profile, the sensitive slice is shifted through the object by decrementing the distance between the surfaces of the sensor and the object in small steps (Figure 1.5c,d). The step size is of the order of the slice thickness. For flat layer structures, the maximum achievable accuracy of measurement has been shown to be 10 µm for an NMR-MOUSE with 5 mm depth range by comparison of nondestructive NMR depth profiles and destructive visual inspection of paint layers with a microscope [21]. For the MiniMOUSE, the maximum resolution is 6 µm [24]. Due to its exceptionally short echo time of less than 20 µs, NMR echo trains can be measured even from rigid materials such as the paint on a car fender (Figure 1.5d,e).

1.2.2.3 Magnets for Bulk-Volume Analysis

Stray-field magnets for bulk volume analysis generate a sweet spot with a sizable volume within which the magnetic field is sufficiently homogeneous to be excited by a radio frequency pulse so that relaxation and diffusion can be measured. An ingenious and simple magnet is the barrel magnet (Figure 1.6a) [30].

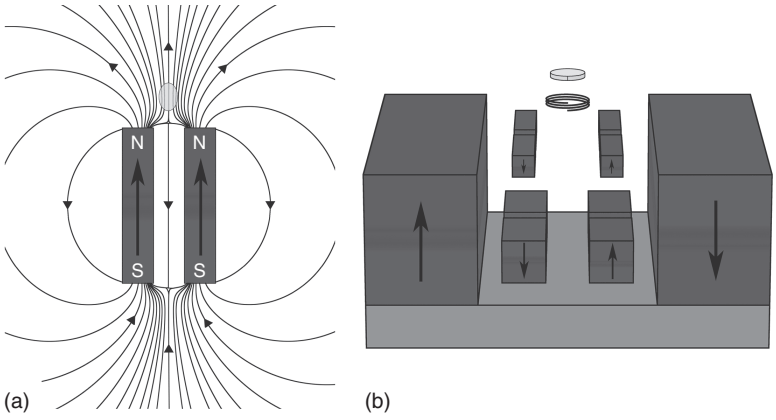

Figure 1.6 Stray-field NMR magnets generating a sweet spot (light grey) external to the top surface of the magnet. (a) Cylindrical barrel magnet. (Fukushima and Jackson 2004 [30]. Reproduced with permission of Elsevier.) The stray field is aligned perpendicular to the magnet surface. (b) NMR-MOUSE with shim magnets generating a homogeneous gradient in a slice. (Van Landeghem *et al*. 2012 [31]. Reproduced with permission of Elsevier.) The stray field is parallel to the magnet surface. The sensitive slice is centered above a RF coil.

This is a hollow cylinder magnetized along the direction of its main axis. Along the axis outside the cylinder, the stray magnetic field passes through a maximum, the position and shape of it can be tailored with the dimensions of the cylinder and by shifting a smaller cylinder magnet inside the bore of the hollow cylinder. A variant of this is the NMR MOLE (MObile Lateral Explorer) [32]. It consists of a circular array of cylinder magnets positioned on a cone. Each magnet is magnetized along its axis, so that the magnets of the MOLE approximate the field lines of the barrel magnet between the face of the barrel and the sweet spot.

For the barrel magnet and the NMR-MOLE, the stray field is oriented perpendicular to the surface of the magnet. Simple current loops generate magnetic fields of similar symmetry, so that they are unsuited as RF coils for such magnets. Instead, two current loops side by side with the current path following the shape of Figure 1.8 are needed to operate such stray-field sensors [23, 30, 32]. With such RF coils, the sensitive volume from which the NMR signal is collected is more difficult to confine than with circular solenoid coils. On the other hand, a sweet spot of the stray field is more difficult to generate when the field is parallel to the magnet surface. Yet it has been shown that the stray field of U-shaped magnets (Figure 1.4c) can be shimmed by displacing smaller magnets inside the magnet gaps, which generate stray fields opposed to the main stray field (Figure 1.6b). The so-called Fourier NMR-MOUSE generates a 2 mm thick slice with a homogeneous gradient of 2 T/m in the direction perpendicular to the sensor surface, so that depth profiles are measured by the principle of frequency encoding from MRI and can be retrieved from the Fourier transform of the echo [21, 31]. In this way, the stray field can even be shimmed locally to sufficient homogeneity to resolve the proton chemical shift for volume-selective NMR spectroscopy of liquids placed in a beaker on top of the magnet [33].

1.2.3 Center-Field Magnets

In contrast to unilateral magnets, center-field magnets generate a sweet spot of the magnetic field inside the magnet assembly. Consequently, the dimensions of the object or the sample have to be smaller than the dimensions of the opening of the magnet. There are two limiting geometries of center-field magnets (Figure 1.7). The classical geometry is the C-shaped magnet with magnetically active poles of equal magnetization, which are separated by a gap that accommodates the sample (Figure 1.7a). Inside the gap, a large volume of magnetic field is established with a low gradient. The return flux from the magnet poles is returned from one pole to the other through an iron yoke. If the iron yoke is on one side, the magnet assumes the shape of a C [9]. Better symmetry is obtained with a two-sided yoke (Figure 1.7b, right) [34]. This geometry has long been in use with electromagnets in the first generation of NMR and ESR spectrometers. Even higher symmetry is obtained, when the two-sided yoke is wrapped around a cylinder to obtain a magnet with axial symmetry (Figure 1.7b, left). This symmetry is only perturbed by small openings to insert the sample and the RF coil (Figure 1.7b, right). Small NMR magnets with magnetic fields sufficiently homogeneous to resolve the ^{1}H chemical shift of solutions contained in capillaries have been built in this way [35]. The field homogeneity may be further improved with accurately shaped iron pole shoes placed on the magnet faces [36].

The other limiting geometry is that of a Halbach magnet (Figure 1.7c) [37]. Following Halbach, center-field magnets can be designed to generate perfect multipolar fields along the axis of an infinitely long cylinder, given that

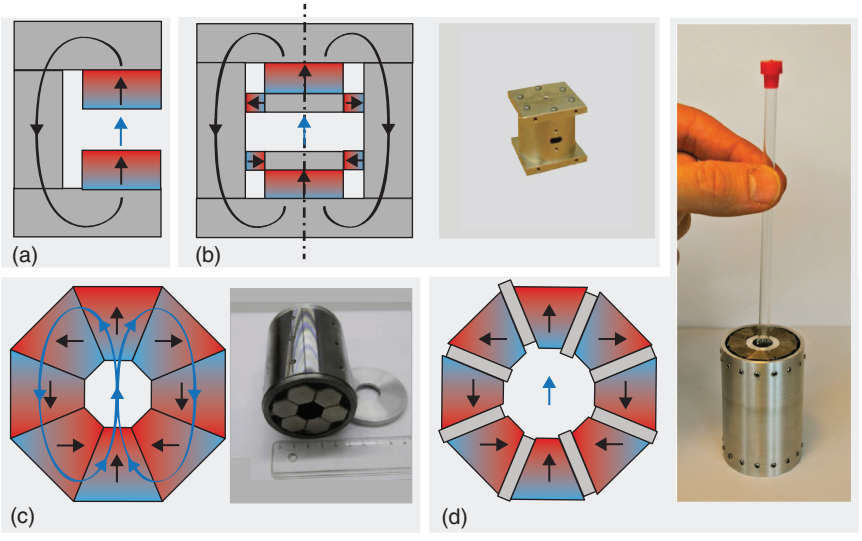

Figure 1.7 Center-field magnets for NMR. These magnets enclose the sample, which has to be inserted into the assembly. (a) Classical C-shaped geometry. (b) Cylinder magnet with an iron housing and iron pole shoes. (c) Halbach magnet from trapezoidal magnet blocks (left). It can be approximated with six identical hexagonal bar magnets magnetized transverse to their axes (right). (d) Halbach magnet with shim plates that can be moved in and out in radial direction.

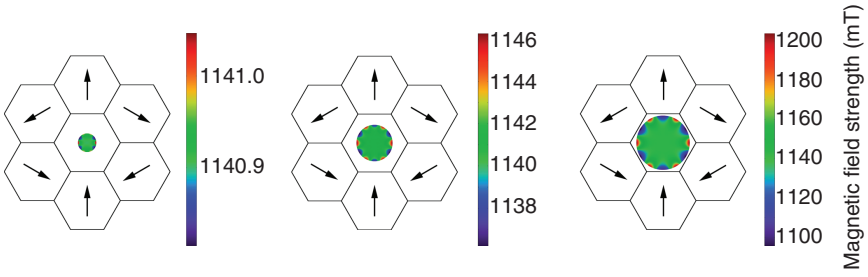

Figure 1.8 Magnetic field strength *B* from finite element numerical simulations evaluated in a circular center plane for three different radii *r*. When the radius is one-third of the inner diameter of the magnet, the variation in the magnetic field is less than 1 mT. By increasing *r* to one-third of the inner diameter and eventually to approximately the bore radius, roughly one order of magnitude is lost in each step.

the magnetization can be generated with annular permanent magnets and infinitesimally small rotations of the magnetization from one volume element to the next within the magnet material. In practice, this condition can only be approximated because the magnet cylinder has to be built with finite length and because it is constructed from individual magnet blocks with finite rotations of the magnetization from one block to the next (Figure 1.7c, left) [38]. A simple way to construct such a magnet is from identical cylinders with a hexagonal cross section, which are magnetized face to face across their diameter (Figure 1.7c, right) [13, 39].

The sample volume in a Halbach magnet is commonly chosen to be one-third of the inner radius or less (Figure 1.8). The field homogeneity achievable across a cross-sectional area is about 10^{-4}, which is about three orders of magnitude inferior to that needed for ^{1}H chemical shift-resolved NMR spectroscopy. The homogeneity of the magnet array needs to be improved by more than one order of magnitude by passive shimming before it can be further improved through active shimming by controlling electrical currents running through wire arrangements. One way to improve the field homogeneity of a Halbach magnet array by passive shimming is to introduce gaps in the array to accommodate displaceable magnet elements (Figure 1.7d, left) [40] or to approximate the Halbach array with cylinder magnets, which can be rotated for shimming [41]. The former approach has been realized with a battery-size magnet for ^{1}H NMR spectroscopy of solutions contained in a standard 5 mm diameter NMR sample tube at 27 MHz (Figure 1.7d, right). Other methods of shimming with magnet elements are described in Section 1.3. As a rule of thumb, the smaller the magnet, the more difficult it is to generate a homogeneous magnetic field.

1.3 Magnet Development

1.3.1 Permanent Magnet Materials

The materials to construct a permanent magnet consist of the magnet block material and the materials of the frame that is holding the blocks in place. The

frame material needs to be strong, light, and nonmagnetic. Suitable materials are fiber-reinforced polymer resins and metals such as aluminum and titanium. The magnet blocks are typically sintered from grains of alloys that contain ferromagnetic iron, cobalt, or nickel. Their properties are characterized by material parameters such as field strength, Curie temperature, temperature coefficient, and homogeneity of the remnant magnetization.

Aluminum–nickel–cobalt (AlNiCo) magnets feature good temperature stability and structural homogeneity while their remnant magnetization is low. Hence their polarization tends to change under the impact of strong external magnetic fields. Samarium–cobalt (SmCo) magnets, on the other hand, exhibit medium field strengths with similar temperature stability and high homogeneity. The highest field strength is obtained with neodymium–iron–boron (NeFeB) magnets. They are readily available and easy to assemble. However, their polarization varies more across their volume than that of AlNiCo or SmCo magnets. Further drawbacks are larger variance in both magnitude and direction of the polarization, lower Curie temperature, and larger temperature coefficient. For protection against corrosion, they are usually coated with nickel. Most permanent NMR magnets are made from either SmCo or NeFeB material with a preference of NeFeB when high field strength has priority.

1.3.2 Magnet Construction and Passive Shimming

A striking development in the development of NMR instruments in recent years was that small and compact NMR devices became available commercially either for dedicated use in diagnostic medicine [11] or as tabletop spectrometers for chemical analysis [3]. Although tabletop NMR relaxometers have been available for a few decades and found to be used in analyzing food and organic materials [42], the big breakthrough came with the availability of compact spectroscopy-grade magnets [43]. Although the commercial compact NMR devices are best classified as tabletop instruments, the vision is to provide handheld NMR devices for medical diagnostic purposes at home and at the bedside, or as monitors in chemical processes and in production lines [44]. A key development goal is therefore the miniaturization [45, 46] of spectroscopy-grade magnets to smaller than the size of a table tennis ball. Some design considerations are addressed in the following text.

1.3.3 Overview of Center-field Magnets for Compact NMR

A variety of different designs for permanent center-field magnets have been published in the literature (Figure 1.9). To compare them in respect to compactness and suitability for spectroscopy, a figure of merit R has been introduced (Table 1.1) [52]:

$$R = (B/\delta)V_S/(m_M V_M) \tag{1.2}$$

which takes into account the field strength B, the relative field homogeneity $\delta = \Delta B/B$, the volume V_S available for the sample, the magnet volume V_M, and the magnet weight m_M. The higher this ratio R is, the better is the quality of the

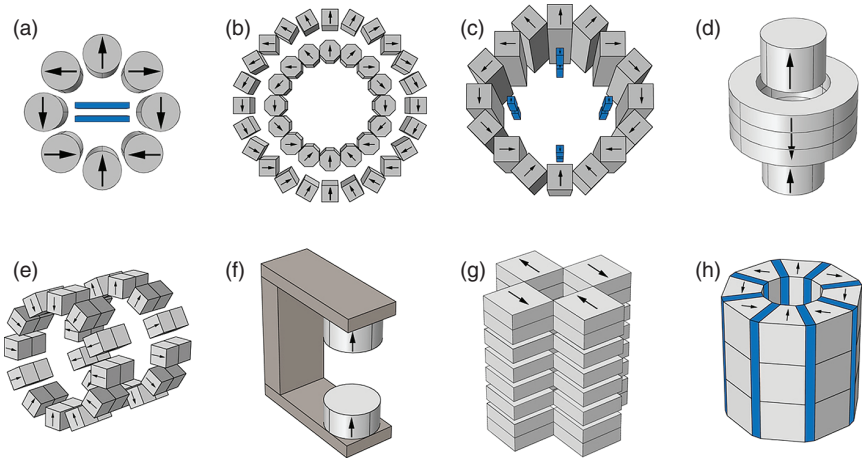

Figure 1.9 Schematic drawings of compact NMR magnets (cf. Table 1.1 for magnet characteristics and literature references). The magnets are referred to by the name of the first author in the publication. (a) Moresi magnet assembled from rotatable cylinder magnets magnetized transverse to their axes. Metal plates (blue) with high permeability further homogenize the field in the center. (Moresi and Magin 2013 [41]. Reproduced with permission of Wiley.) (b) Armstrong magnet with tunable field strength. It is assembled from two Halbach magnets that can be rotated against each other. (Armstrong *et al*. 2008 [47]. Reproduced with permission of Elsevier.) (c) Danieli magnet I. It is a Halbach magnet for magnetic resonance imaging similar to one ring of the Armstrong magnet but with shim magnets (blue) in the center. (Danieli *et al*. 2009 [48]. Reproduced with permission of Elsevier.) (d) Manz magnet approximating a simple spherical Halbach magnet. (Manz *et al*. 2008 [49]. Reproduced with permission of Elsevier.) (e) Hugon magnet, which produces a magnetic field aligned with the direction of the magnet bore. (Hugon *et al*. 2010 [50]. Reproduced with permission of Elsevier.) (f) Sun magnet with the smallest dimensions of all magnets shown. (g) Windt magnet, better known as the NMR-CUFF, which can be opened and closed to fit around a long pipe or a plant stem. (Windt *et al*. 2011 [51]. Reproduced with permission of Elsevier.) (h) Danieli magnet II, a Halbach magnet from trapezoidal magnet elements with shim plates (blue) that can be moved for shimming. This design yields the highest figure of merit. (Danieli *et al*. 2010 [40]. Reproduced with permission of Wiley.)

Table 1.1 Compact permanent magnets and their characteristic summarized in a figure of merit *R*.

Author	B (T)	δ (ppm)	V_S (cm^3)	V_M (cm^3)	m_M (kg)	R (T/kg)
Moresi [41]	0.60	10	0.045	5853	7	0.07
Armstrong [47]	0.45	20	1.571	4396	32	0.25
Danieli I [48]	0.22	11	21.206	23093	50	0.38
Manz [49]	1.00	50	0.003	205	0.6	0.52
Hugon [50]	0.12	10	0.042	512	1.8	0.55
Sun [9]	0.56	50	0.001	11	0.7	1.42
Windt [51]	0.57	50	0.196	128	3.1	5.64
Danieli II [40]	0.70	0.15	0.196	308	0.5	5.95×10^3

magnet as a compact device. The highest rating receives the Halbach magnet (Figure 1.7d) built from trapezoidal magnet elements separated by adjustable magnet plates for shimming [40]. Yet for handheld devices exploring NMR spectroscopy, this magnet is still too large so that further magnet miniaturization is required and other concepts need to be explored.

1.3.4 Strategies for Passive Shimming

When aiming at the construction of small spectroscopy-grade center-field magnets in terms of an array from individual magnet elements, different concepts are followed to improve the homogeneity of the field in the center. A basic and straightforward approach is to accept imperfections of the magnet elements in dimension, polarization magnitude, and direction as given and find ways to produce a magnetic field sufficiently homogeneous for spectroscopy in the magnet center. One way is to carefully adjust the positions of individual magnet elements in the array. For shimming, a subset of small, dedicated magnets can be moved near the center, taking space away otherwise available for active shims and the sample (Figure 1.9c) [48]. This cost in magnet volume is avoided when magnetic plates are introduced in gaps between parallel walls of the main magnet assembly that can precisely be displaced (Figure 1.9h) [40].

A conceptually different approach to generate a highly homogeneous center field is the pursuit of perfection of the magnetic material and the magnet assembly. This approach has led to the development of the first semipermanent high-field magnet from magnetized, superconducting material grown as single-crystal rings [53]. Pushed to the extreme, the underlying philosophy would be to grow the magnet from atoms, possibly into an optimized shape, with precision on the atomic-level reminiscent of 3D printing, where an object is constructed via the controlled deposition of molecules. At the other extreme, an imperfect magnet could be shimmed by ablation with atomic precision to reduce the overall effect of imperfections on the homogeneity of the field. High-precision ablation can be achieved with lasers and electron beams, which at the same time can manipulate the remnant polarization by local heating of the material surface above the Curie temperature [54].

A third way of passive shimming intermediate to the two extremes discussed so far is to exploit the imperfections of the components of the magnet array for improving the magnetic field homogeneity [38]. Relative variations in magnetic polarization and dimensions of permanent magnet elements are typically of the order 1%. These variations can be determined for each element and constructively put to use to improve the homogeneity in the center of the array. This has been demonstrated with Halbach rings assembled from hexagonal magnet blocks (Figure 1.8) in a computer simulation study employing genetic algorithms [52].

Center-field magnets following the Halbach design [37] are popular for NMR because the magnetic field is transverse to the axis of the bore so that solenoidal

coils can be employed for detection of the nuclear induction signal instead of less sensitive saddle coils. The ideal Halbach magnet is infinitely long. In practice, axial inhomogeneity from finite length is reduced by composing a Halbach magnet from two or more rings spaced a critical distance apart that minimizes the axial field inhomogeneity [38, 48]. However, there is still a finite transverse inhomogeneity resulting from the finite number of elements in the ring [55]. Typically, this inhomogeneity is of the order of 10^{-4} even for up to 18 perfect finite-size elements [52], whereas less than 10^{-6} is required for ^{1}H NMR spectroscopy.

Conceptually the simplest way to build Halbach magnets is from hexagonal rods (Figures 1.7c, right and 1.8) [13, 39]. The field obtained from two shells of perfect hexagonal bars may further be shimmed by placing identical magnets into a third shell. This has been simulated employing a genetic algorithm to find the best out of 10^{15} possible configurations (Figure 1.10a) [52]. It turns out that better homogeneity can be achieved, when the core shim unit from 18 hexagonal elements is built from flawed bar magnets with random imperfections in the overall polarization magnitude of the order of 1% and then shimmed with perfect elements (Figure 1.10b). The game-changing message in this study is that magnet imperfections can be made use of for improving the field homogeneity beyond that which is expected for a construction of a Halbach magnet with perfect elements.

1.3.5 Shim Coils for Compact NMR Magnets

Once the homogeneity of a magnet is of the order of 10 ppm or better, it can be further improved by active shimming with the magnetic fields from current-driven wire arrangements [56]. There are three conceptually different approaches suitable for compact permanent magnets. Active shims have the advantage of adjusting the field homogeneity without the need of moving magnets or other parts in the magnet array.

The traditional way of actively eliminating residual magnetic field inhomogeneity was invented by Anderson [57]. He expanded the inhomogeneous magnetic field into spherical harmonics and designed sets of coils for a C-shaped electromagnet that produce magnetic field components matching the orthogonal terms of the expansion (Figure 1.11a). The current flow though these sets can independently be adjusted to compensate the gradient field of the magnet. Although in theory, the field terms produced by the shim coils are orthogonal, in practice cross-terms cannot be avoided, so that shimming becomes an iterative process [58] that today can be automized and left completely under computer control [59].

A fundamentally different approach was implemented by the team of Kose [60] who used an array of small circular coils aligned on a regular lattice (Figure 1.11b). The current through each coil is adjusted individually to shim the magnetic field. Temperature drifts of the magnet can be compensated by providing a suitable bias current to all coil elements in the array. This type of shimming necessitates

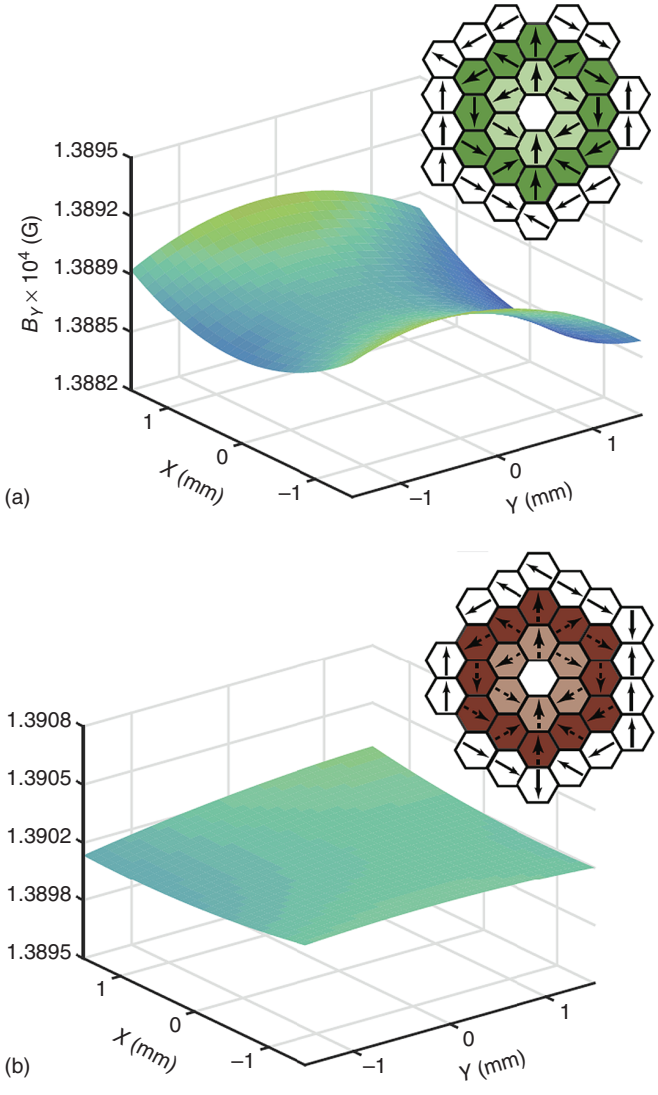

Figure 1.10 Simulated field maps of Halbach magnets constructed from hexagonal bar magnets (Adapted from [52].) and shimmed with ideal bar magnets placed in the third shell. (a) Halbach magnet with the inner two shells constructed from ideal magnet elements. (b) Halbach magnet with the inner two shells constructed from flawed magnet elements.

use of computer algorithms to set the currents in each coil of the array because the field contributions from one coil are not even approximately orthogonal to those of the others. This concept has been extended by McDowell to crossing straight wires instead of neighboring current loops in an effort to downsize the volume of the shim unit (Figure 1.11c) [61].

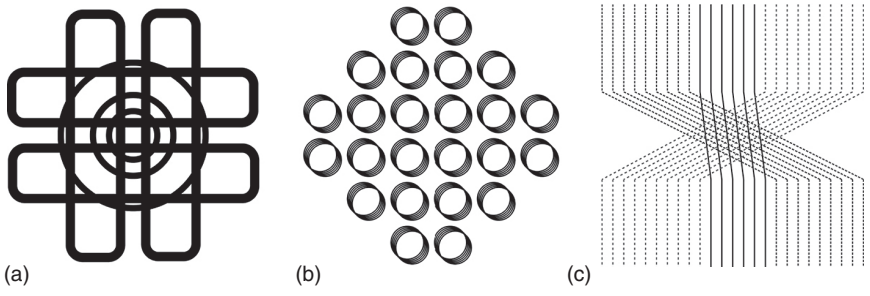

Figure 1.11 Approaches for active shimming of C-shaped magnets. (a) The Anderson method employs sets of coils that produce magnetic field contributions following the terms of an expansion of the field variation in spherical harmonic functions. (b) The Kose method employs a two-dimensional array of individually driven ring currents. (c) The McDowell method employs the magnetic fields from current-driven individual wires crossing each other in parallel arrays.

1.4 Concluding Remarks

The trend to miniaturize NMR hardware began with the introduction of microcoils at high field [62] and with the introduction of mobile magnets at low field for tabletop relaxometry [63], well-logging [64], and nondestructive testing [15, 64]. Along with the advances in miniaturization of consumer electronics, the introduction of the cellphone, and fitness trackers, the vision of personalized NMR devices for materials testing such as moisture sensing [27] and for point-of-care diagnostics gains momentum [65]. Such medical devices could employ small stray-field magnets for skin diagnostics or small center-field magnets for relaxometric and spectroscopic analyses [46] of body fluids processed with lab-on-a chip technology and hyperpolarized with *para*-hydrogen spin order [66, 67], by transfer of electron magnetization through dynamic nuclear polarization [68], or by transfer from optically polarized nitrogen vacancy centers in diamond [69]. One of the challenging key elements in this scenario is a small magnet with a large sample volume and a highly homogeneous field. Although a road leading in this direction has been mapped out with the recent advent of tabletop high-resolution NMR spectrometers [3], challenges remain in making temperature-stable, pingpong-ball size, permanent magnets with sub-ppm resolution for chemical identification. This overview is an attempt to summarize the state of the art and some design principles in an effort to assist the development of such magnets. It appears that most of the puzzle pieces to reach this goal are being collected and the puzzle is about to be put completed.

References

1 Abragam, A. (1961) *The Principles of Nuclear Magnetism*, Clarendon Press, Oxford.
2 Slichter, C.P. (1990) *Principles of Magnetic Resonance*, Springer, Berlin.
3 Blümich, B. (2016) Introduction to compact NMR: a review of methods. *TrAC, Trends Anal. Chem.*, **83**, 2–11.

4 Wüthrich, K. (1986) *NMR of Proteins and Nucleic Acids*, Wiley-Interscience, Hoboken.

5 Danieli, E., Blümich, B., and Casanova, F. (2012) Mobile nuclear magnetic resonance, in *eMagRes* (eds R.K. Harris and R.E. Wasylishen), John Wiley & Sons, Ltd, Chichester.

6 Blümich, B., Haber-Pohlmeier, S., and Zia, W. (2014) *Compact NMR*, de Gruyter, Berlin.

7 Johns, M., Fridjonson, E.I., Vogt, S., and Haber, A. (2016) *Mobile NMR and MRI*, Royal Society of Chemistry, Cambridge.

8 Sillerud, L.O., McDowell, A.F., Adolphi, N.L., Serda, R.E., Adams, D.P., Vasile, M.J., and Alam, T.M. (2006) ^{1}H NMR detection of superparamagnetic nanoparticles at 1 T using a microcoil and novel tuning circuit. *J. Magn. Reson.*, **181**, 181–190.

9 Sun, N., Yoon, T.-J., Lee, H., Andress, W., Weissleder, R., and Ham, D. (2011) Palm NMR and 1-Chip NMR. *IEEE J. Solid-State Circuits*, **46**, 342–352.

10 Sun, N., Liu, Y., Qin, L., Lee, H., Weissleder, R., and Ham, D. (2013) Small NMR biomolecular sensors. *Solid-State Electron.*, **84**, 13–21.

11 Neely, L.A., Audeh, M., Phung, N.A., Min, M., Suchocki, A., Plourde, D., Blanco, M., Demas, V., Skewis, L.R., Anagnostou, T., Coleman, J.J., Wellman, P., Mylonakis, E., and Lowrey, T.J. (2013) T2 magnetic resonance enables nanoparticle-mediated rapid detection of candidemia in whole blood. *Sci. Transl. Med.*, **5**, 182ra54.

12 Peng, W.K., Kong, T.F., Ng, C.S., Chen, L., Huang, Y., Bhagat, A.A.S., Nguyen, N.-T., Preiser, P.R., and Han, J. (2014) Micromagnetic resonance relaxometry for rapid label-free malaria diagnosis. *Nat. Med.*, **20**, 1069–1073.

13 Blümich, B., Casanova, F., and Appelt, S. (2009) NMR at low magnetic fields. *Chem. Phys. Lett.*, **477**, 231–240.

14 Eidmann, G., Savelsberg, R., Blümler, P., and Blümich, B. (1996) The NMR MOUSE: a mobile universal surface explorer. *J. Magn. Reson., Ser. A*, **122**, 104–109.

15 Blümich, B., Perlo, J., and Casanova, F. (2008) Mobile single-sided NMR. *Prog. Nucl. Magn. Reson. Spectrosc.*, **52**, 197–269.

16 Suefke, M., Liebisch, A., Blümich, B., and Appelt, S. (2015) External high-quality-factor resonator tunes up nuclear magnetic resonance. *Nat. Phys.*, **11**, 767–771.

17 Casanova, F., Perlo, J., and Blümich, B. (2011) *Single-sided NMR*, Springer, Berlin.

18 Marble, A.E., Mastikhin, I.V., Colpitts, B.G., and Balcom, B.J. (2007) A compact permanent magnet array with a remote homogeneous field. *J. Magn. Reson.*, **186**, 100–104.

19 Kleinberg, R.L., Sezginer, A., Griffin, D.D., and Fukuhara, M. (1992) Novel NMR apparatus for investigating an external sample. *J. Magn. Reson.*, **97**, 466–485.

20 Demas, V. and Prado, P.J. (2009) Compact magnets for magnetic resonance. *Concepts Magn. Reson. Part A*, **34**, 48–59.

21 Perlo, J., Casanova, F., and Blümich, B. (2005) Profiles with microscopic resolution by single-sided NMR. *J. Magn. Reson.*, **176**, 64–70.

22 Danieli, E., Blümich, B., and Casanova, F. (2014) Mobile NMR, in *NMR Spectroscopy: A Versatile Tool for Environmental Research* (eds M.J. Simpson and A.J. Simpson), John Wiley & Sons, Inc, New York, pp. 149–165.

23 Blümler, P. and Casanova, F. (2016) Hardware developments: single-sided magnets, in *Mobile NMR and MRI* (eds M. Johns, E.O. Fridjonson, S. Vogt, and A. Haber), Royal Society of Chemistry, Cambridge, pp. 110–132.

24 Oligschläger, D., Glöggler, S., Watzlaw, J., Brendel, K., Jaschtschuk, D., Colell, J., Zia, W., Vossel, M., Schnakenberg, U., and Blümich, B. (2015) A miniaturized NMR-MOUSE with a high magnetic field gradient (mini-MOUSE). *Appl. Magn. Reson.*, **46**, 181–202.

25 Casanova, F. and Blümich, B. (2003) Two-dimensional imaging with a single-sided NMR probe. *J. Magn. Reson.*, **163**, 38–45.

26 Casanova, F., Perlo, J., and Blümich, B. (2004) Velocity distributions remotely measured with a single-sided NMR sensor. *J. Magn. Reson.*, **17**, 124–130.

27 Oligschläger, D., Kupferschläger, K., Poschadel, T., Watzlaw, J., and Blümich, B. (2014) Miniature mobile NMR sensors for material testing and moisture-monitoring. *Diffus. Fundam.*, **22**, 1–25.

28 Oligschläger, D., Lehmkuhl, S., Watzlaw, J., Benders, S., de Boever, E., Rehorn, C., Vossel, M., Schnakenberg, U., and Blümich, B. (2015) Miniaturized multi-coil arrays for functional planar imaging with a single-sided NMR sensor. *J. Magn. Reson.*, **254**, 10–18.

29 Watzlaw, J., Glöggler, S., Blümich, B., Mokwa, W., and Schnakenberg, U. (2013) Stacked planar micro coils for single-sided NMR applications. *J. Magn. Reson.*, **230**, 176–185.

30 Fukushima, E. and Jackson, J.A. (2004) Unilateral magnet having a remote uniform field region for nuclear magnetic resonance. US6489872, published Dec. 3, 2002; US6828892 published Dec. 7, 2004; Fukushima, E. and Utsuzawa, S., (2017) Unilateral NMR with a barrel magnet, *J. Magn. Reson.*, **282**, 104–113.

31 Van Landeghem, M., Danieli, E., Perlo, J., Blümich, B., and Casanova, F. (2012) Low-gradient single-sided NMR sensor for one-shot profiling of human skin. *J. Magn. Reson.*, **215**, 74–84.

32 Manz, B., Coy, A., Dykstra, R., Eccles, C.D., Hunter, M.W., Parkinson, B.J., and Callaghan, P.T. (2006) A mobile one-sided NMR sensor with a homogeneous magnetic field: the NMR-MOLE. *J. Magn. Reson.*, **183**, 25–31.

33 Perlo, J., Demas, V., Casanova, F., Meriles, C.A., Reimer, J., Pines, A., and Blümich, B. (2005) High-resolution NMR spectroscopy with a portable single-sided sensor. *Science*, **308**, 1279.

34 Sahebjavaher, R.S., Walus, K., and Stoeber, B. (2010) Permanent magnet desktop magnetic resonance imaging system with microfabricated multiturn gradient coils for microflow imaging in capillary tubes. *Rev. Sci. Instrum.*, **81**, 023706.

35 McDowell, A. and Fukushima, E. (2008) Ultracompact NMR: ^{1}H spectroscopy in a subkilogram magnet. *Appl. Magn. Reson.*, **35**, 185–195.

36 Ryu, J.S., Yao, Y., Koh, C.S., and Shin, Y.J. (2006) 3-D optimal shape design of pole piece in permanent magnet MRI using parameterized nonlinear design sensitivity analysis. *IEEE Trans. Magn.*, **42**, 1351–1354.

37 Halbach, K. (1980) Design of permanent multipole magnets with oriented rare earth cobalt material. *Nucl. Instrum. Methods*, **169**, 1–10.

38 Soltner, H. and Blümler, P. (2010) Dipolar Halbach magnet stacks made from identically shaped permanent magnets for magnetic resonance. *Concepts Magn. Reson.*, **A36**, 211–222.

39 Blümich, B., Mauler, J., Haber, A., Perlo, J., Danieli, E., and Casanova, F. (2009) Mobile NMR for geophysical analysis and materials testing. *Pet. Sci.*, **6**, 1–7.

40 Danieli, E., Perlo, J., Blümich, B., and Casanova, F. (2010) Small magnets for portable NMR spectrometers. *Angew. Chem. Int. Ed.*, **49**, 4133–4135.

41 Moresi, G. and Magin, R. (2003) Miniature permanent magnet for table-top NMR. *Concepts Magn. Reson. Part B*, **19B**, 35–43.

42 Barker, P.J. and Stronks, H.J. (1990) Application of the low resolution pulsed NMR "Minispec" to analytical problems in the food and agriculture industries, in *NMR Applications in Biopolymers* (eds J.W. Finley, S.J. Schmidt, and A.S. Serianni), Springer US, Boston.

43 Blümler, P. and Casanova, F. (2016) Hardware developments: Halbach magnet arrays, in *Mobile NMR and MRI* (eds M. Johns, E.O. Fridjonson, S. Vogt, and A. Haber), Royal Society of Chemistry, Cambridge, pp. 133–157.

44 Haun, J.B., Castro, C.M., Wang, R., Peterson, V.M., Marinelli, B.S., Lee, H., and Weissleder, R. (2011) Micro-NMR for rapid molecular analysis of human tumor samples. *Sci. Transl. Med.*, **3**, 71ra16.

45 Zalesskiy, S.S., Danieli, E., Blümich, B., and Ananikov, V.P. (2014) Miniaturization of NMR systems: desktop spectrometers, microcoil spectroscopy, and "NMR on a chip" for chemistry, biochemistry, and industry. *Chem. Rev.*, **114**, 5641–5694.

46 Ha, D., Paulsen, J., Sun, N., Song, Y.-Q., and Ham, D. (2014) Scalable NMR Spectroscopy with Semiconductor Chips. *Proc. Natl. Acad. Sci. U.S.A.*, **111**, 11955–11960.

47 Armstrong, B.D., Lingwood, M.D., McCarney, E.R., Brown, E.R., Blümler, P., and Han, S.-I. (2008) Portable X-band system for solution state dynamic nuclear polarization. *J. Magn. Reson.*, **191**, 273–281.

48 Danieli, E., Mauler, J., Perlo, J., Blümich, B., and Casanova, F. (2009) Mobile sensor for high resolution NMR spectroscopy and imaging. *J. Magn. Reson.*, **198**, 80–87.

49 Manz, B., Benecke, M., and Volke, F. (2008) A simple, small and low cost permanent magnet design to produce homogeneous magnetic fields. *J. Magn. Reson.*, **192**, 131–138.

50 Hugon, C., D'Amico, F., Aubert, G., and Sakellariou, D. (2010) Design of arbitrarily homogeneous permanent magnet systems for NMR and MRI: theory and experimental developments of a simple portable magnet. *J. Magn. Reson.*, **205**, 75–85.

51 Windt, C.W., Soltner, H., van Dusschoten, D., and Blümler, P. (2011) A portable Halbach magnet that can be opened and closed without force: the NMR-CUFF. *J. Magn. Reson.*, **208**, 27–33.

52 Parker, A.J., Zia, W., Rehorn, C.W.G., and Blümich, B. (2016) Shimming Halbach magnets utilizing genetic algorithms to profit from material imperfections. *J. Magn. Reson.*, **265**, 83–89.

53 Ogawa, K., Nakamura, T., Terada, Y., Kose, K., and Haishi, T. (2011) Development of a magnetic resonance microscope using a high bulk superconducting magnet. *Appl. Phys. Lett.*, **98**, 234101.

54 Danieli, E.P., Blümich, B., Zia, W., and Leonards, H. (2015) Method for a targeted shaping of the magnetic field of permanent magnets. WO 2015043684 A1 pending, published 2.

55 Turek, K. and Liszkowski, P. (2014) Magnetic field homogeneity perturbations in finite Halbach dipole magnets. *J. Magn. Reson.*, **238**, 52–62.

56 Wachowicz, K. (2014) Evaluation of active and passive shimming in magnetic resonance imaging. *Res. Rep. Nucl. Med.*, **4**, 1–12.

57 Anderson, W.A. (1961) Electrical current shims for correcting magnetic fields. *Rev. Sci. Instrum.*, **32**, 241–250.

58 Chmurny, G.N. and Hoult, D.I. (1990) The ancient and honourable art of shimming. *Concepts Magn. Reson.*, **2**, 131–149.

59 Terada, Y., Ishi, K., Tamada, D., and Kose, K. (2013) Power optimization of a planar single-channel shim coil for a permanent magnet circuit. *Appl. Phys Express*, **6**, 026701.

60 Terada, Y., Kono, S., Ishizawa, K., Inamura, S., Uchiumi, T., Tamada, D., and Kose, K. (2013) Magnetic field shimming of a permanent magnet using a combination of pieces of permanent magnets and a single-channel shim coil for skeletal age assessment of children. *J. Magn. Reson.*, **230**, 125–133.

61 Leskowitz, G.M., McFeetors, G., and Pernecker, S. (2014) Method and apparatus for producing homogeneous magnetic fields. US8712706, published 29.

62 Olson, D.L., Peck, T.L., Webb, A.G., Magin, R.L., and Sweedler, J.V. (1995) High-resolution microcoil ^{1}H-NMR for mass-limited, nanoliter-volume samples. *Science*, **270**, 1967–1970.

63 van Putte, K. and van den Enden, J. (1974) Fully automated determination of solid Fat content by pulsed NMR. *J. Am. Oil Chem. Soc.*, **51**, 316–320.

64 Jackson, J.A., Burnett, L.J., and Harmon, F. (1980) Remote (inside-out) NMR. III. Detection of nuclear magnetic resonance in a remotely produced region of homogeneous magnetic field. *J. Magn. Reson.*, **41**, 411–421.

65 Issadore, D. and Westervelt, R.M. (eds) (2013) *Point-of-Care Diagnostics on a Chip*, Springer, Heidelberg.

66 Prina, I., Buljabasich, L., and Acosta, R.H. (2015) Parahydrogen discriminated PHIP at low magnetic fields. *J. Magn. Reson.*, **251**, 1–7.

67 Spannring, P., Reile, I., Emondts, M., Schleker, P.P.M., Hermkens, N.K.J., van der Zwaluw, N.G.J., van Weerdenburg, B.J.A., Tinnemans, P., Tessari, M., Blümich, B., Rutjes, F.P.J.T., and Feiters, M.C. (2016) A new Ir-NHC-catalyst for signal amplification by reversible exchange in D_2O, *Chem. Eur. J.*, **2016**, 9277–9282.

68 Halse, M.E. (2016) Perspectives for hyperpolarization in compact NMR. *Trends Anal. Chem.*, **83**, 76–83.

69 Scott, E., Drake, M., and Reimer, J.A. (2016) The phenomenology of optically pumped ^{13}C NMR in diamond at 7.05 T: Room temperature polarization, orientation dependence, and the effect of defect concentration on polarization dynamics. *J. Magn. Reson.*, **264**, 154–162.